INVESTIGATING MORPHOMETRIC CHARACTERISTICS OF SHORTENING STRUCTURES ACROSS MARS. Rachel M. Atkins[1], Paul K. Byrne[1] and DelWayne R. Bohnenstiehl[1] [1]Department of Marine, Earth, and Atmospheric Sciences, North Carolina State University, Raleigh, NC 27695, USA (ratkins@ncsu.edu).

Introduction: The Martian surface shows evidence for a long history of compressional tectonism in the form of wrinkle ridges and lobate scarps, the main differences between the two features being their cross-sectional symmetry and scale [1–3]. Lobate scarps are asymmetric, positive-relief landforms with a steep front scarp and gently-sloping back scarp (Fig. 1) [4]. Evidence from compressional scarps on Earth indicates that these landforms are produced via large thrust faults producing an overlying antiformal fault-propagation fold (i.e., the surface scarp) [5,6]. Their widespread distribution on Mars suggests global contraction as a leading formation mechanism [7].

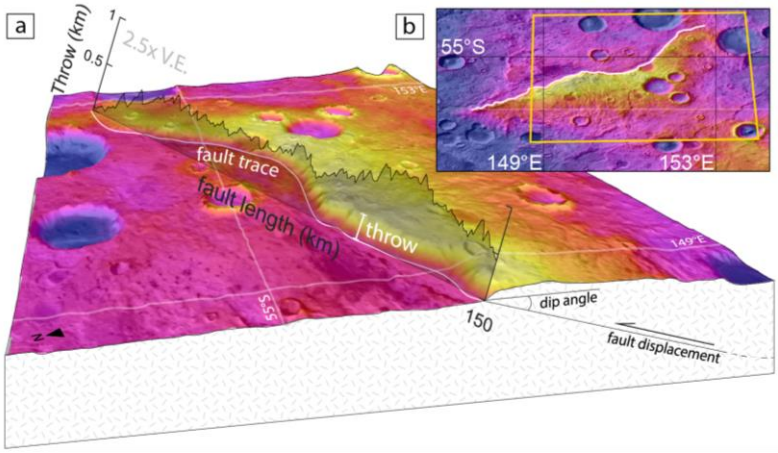

Figure 1. (a) 3-dimensional diagram of fault trace with extracted throw profile and calculated metrics; (b) overview of this example fault, which is in the southern hemisphere.

Where fault displacements cannot be directly measured, as is the case for buried Terran faults [8,9] and those on other planetary bodies such as Mercury and Mars [10,11], surface morphology can be taken as a proxy for fault geometry; indeed, changes in surface displacement along the length of a fault provides insight into fault growth history, the extent of fault linkage, and even the thickness of the brittle layer in which the fault formed [12,13].

Studies of Terran faults indicate that the relationship between maximum fault displacement (D_{max}) and fault length (L) for faults in a given population is quasi-linear [e.g., 12]. Deviations from this relationship can reveal impediments to fault growth such as mechanical restrictions of fault penetration at depth, and fault segment linkage when D_{max}/L ratios are lower than expected [13,14]. Alternatively, ratios that are higher than expected can indicate more fault displacement is being accommodated than is predicted for a given fault length, possibly indicating restriction on lateral fault propagation [15]. This work aims to determine D_{max}/L for a population of globally distributed thrust faults on Mars, as well as characterize the extent of fault segmentation—the combination of which can provide insights for fault evolution and brittle layer thicknesses.

Methods: Thrust-fault-related scarps on Mars were identified in ArcGIS by their curvilinear shape and asymmetry orthogonal to strike in map-view, using the MOLA–HRSC blended digital elevation model (200 m/px) combined with THEMIS imagery (100 m/px). Of a total of 143 landforms, we downselected 49 based on their: (1) relative spatial isolation from adjacent uplifts; (2) lack of large (>50 km diameter) impact craters that could affect surface displacement measurements; and (3) geographic dispersion across the planet.

Displacement profiles were constructed by taking scarp-normal topographic transects at 1-km intervals to measure maximum surface displacement along the scarp, which we take as fault throw (assuming minimal erosion). Once maximum throw (t) values were determined, D_{max} was calculated by $D_{max} = t/\sin(\alpha)$, where α is an assumed planar fault dip angle. Forward models of Martian thrust faults predict fault dip angles of 15–40° [e.g., 16], which is consistent with observations of Terran thrusts. Therefore, and to maintain consistency with recent studies that reported D_{max}/L data for select structures on Mars [11], we used a fault dip angle of 30° for this work.

Displacement profile shapes were also characterized as elliptical or triangular to assess fault growth, and particularly to look for evidence of symmetric or asymmetric growth (i.e., involving fault linkage). We applied fast Fourier transform (FFT) and S-Transform (ST) spectral analyses to quantify variance in along-strike fault displacement, following approaches developed by Manighetti et al. [17] for Terran faults.

Fault displacement profiles were first assessed by subtracting the dominant shape that best represented each profile from displacement values along its length (Fig. 2). The spectral analyses were then used to characterize spectral amplitude (i.e., fault displacement) as a function of spatial frequency (i.e., fault length). For example, a fault with a spatial frequency of two cycles corresponds to a fault profile exhibiting two dominant

segments with distinct peaks in slip displacement. The major differences between the FFT and ST calculations are that the former technique considers fixed segment lengths, whereas the latter allows for variable segment lengths. Combining both of these methods, and assessing how they agree both with each other and with the photogeological evidence for segmentation, allows for the quantification of segmentation in this population.

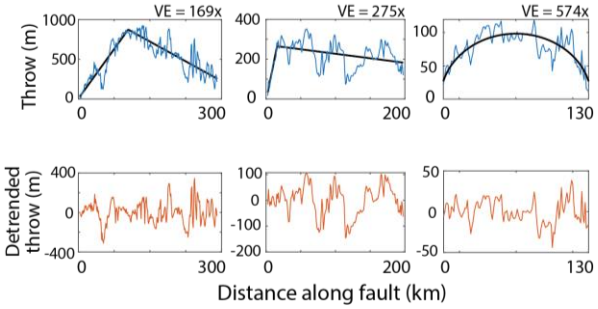

Figure 2. Three example faults with best-fit shapes (top row) used to assess profiles. Three example faults shown here display slightly and substantially skewed triangle fits (left and middle, respectively) and a symmetrical elliptical fit for spectral analysis (right). Detrended profiles (bottom row).

Findings: Of the 49 faults investigated, their lengths ranged from 34 km to 544 km, with maximum scarp heights of 85 m to 2.1 km. Assuming a planar fault geometry and a fault dip of 30°, these structures have an average D_{max}/L of $6.1\times10^{-3} \pm 1.4\times10^{-3}$, which falls within the published ranges for other Martian thrust faults [e.g., 3,4,18,19]. Significantly (p <0.001) lower ratios were found for the northern lowlands ($2.9\times10^{-3} \pm 0.9\times10^{-3}$) than the southern highlands ($9.2\times10^{-3} \pm 1.9\times10^{-3}$). The FFT and ST analyses returned generally similar fault segmentation results, particularly for faults with greater than five segments.

The D_{max}/L and segmentation results reveals an inverse relationship between that scaling ratio and segmentation number (Fig. 3). The lower calculated D_{max}/L for thrusts in the northern lowlands reveal that less displacement is accommodated for a given length by faults there than in the southern uplands. If these differences in fault behavior are a function of hemispherical differences in brittle lithospheric thickness, our findings require a thinner lithosphere in the north. Current lithosphere models , however, suggest the thinner northern crust actually leads to a thicker lithosphere there [e.g., 20,21]. The timing of fault initiation (i.e., the history of strain accumulation) could account for these D_{max}/L differences, although there is little evidence at present for faults in the north having initiated later and thus exhibiting lower levels of maturity than their southern counterparts. Alternatively, differences in the geometry of northern thrusts (e.g., ramp-flat, listric, and/or shallower faults compared with steeper, homoclinal structures in the southern uplands)—perhaps reflecting the presence of interbedded, layered units in the lowlands—may explain these hemispherical differences in shortening strains [e.g., 22].

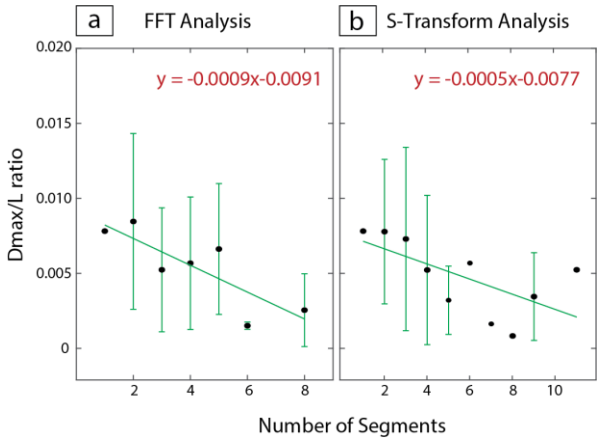

Figure 3. D_{max}/L *vs segmentation relationships for both spectral analyses. Both regressions (red text) are significant (p <0.05).*

Outlook: Investigating the relative and absolute model ages of these structures with crater statistics offers a means to test whether differences in D_{max}/L between faults in the southern uplands and northern lowlands is explained by differences in the timing of fault initiation. Results from timing analyses may also provide additional insight about the stratigraphic properties of the northern and southern portions of the Martian lithosphere.

References: [1] Mueller K. and Golombek M. (2004) *Annu. Rev. of Earth and Planet. Sci. 32*, 435-464. [2] Solomon S. C. (1978) *Geophysical Research Letters, 5*, 461–464. [3] Watters T. R. (2004) *Icarus, 171*, 284-294. [4] Watters T. R. and Robinson M. S. (1999) *JGR, 104*, 981-990. [5] Suppe, J. and Medwedeff, D. (1990) *Eclogae Geologicae Helvetiae, 454*, 409–454. [6] Wickham, J. (1995) *Journal of Structural Geology, 17*, 1293–1302. [7] Schubert G. and Spohn T. (1990) *JGR, 95*, 95-104. [8] Kim Y. and Sanderson D. J. (2005) *Earth Science Reviews, 68*, 317-334. [9] Davis K. et al. (2005) *Journal of Structural Geology, 27*, 1528-1546. [10] Byrne P. K. et al. (2014) *Nature Geoscience, 7*, 301–307. [11] Klimczak, C. et al. (2018) *JGR Planets, 123*, 1973–1995. [12] Cowie, P. and Scholz, C. (1992) *Journal of Structural Geology, 14*, 1149–1156. [13] Dawers N. H. and Anders M. H. (1995) *Journal of Structural Geology, 17*, 607-614. [14] Cartwright J. A. et al. (1995) *Journal of Structural Geology, 17*, 1319-1326. [15] Nicol A. et al. (1996) *Journal of Structural Geology, 18*, 235-248. [16] Egea-Gonzalez I. et al. (2017) *Icarus, 288*, 53-68. [17] Manighetti I. et al. (2009) *Earth and Planetary Science Letters, 288*, 370-381. [18] Schultz R. et al. (2006) *Journal of Structural Geology, 28*, 2182–2193. [19] Ruj T. et al. (2018) *Geoscience Frontiers, 10*, 1029-1037. [20] Montesi L. and Zuber M. (2003) *Journal of Geophysical Research, 108*, 1-25. [21] Jimenez-Diaz A. et al. (2021) *Icarus, 353*. [22] Polit A. T. et al. (2009) *Journal of Structural Geology, 31*, 662-673.